Nuclear Inst. and Methods in Physics Research, A 1032 (2022) 166627

Contents lists available at ScienceDirect

Nuclear Inst. and Methods in Physics Research, A

journal homepage: www.elsevier.com/locate/nima

The CMS MTD Endcap Timing Layer: Precision timing with Low Gain Avalanche Diodes

M. Ferrero, on behalf of the CMS Collaboration

Università Del Piemonte Orientale, Italy

ARTICLE INFO

Keywords:
CMS MTD
LGAD

ABSTRACT

The MIP Timing Detector of the CMS detector will provide precision timestamps with 40 ps resolution for all charged particles up to a pseudorapidity of $|\eta| = 3.0$. This upgrade will mitigate the effects of pile-up expected under the High-Luminosity LHC running conditions and bring new and unique capabilities to the CMS detector. The endcap region of the MIP Timing Detector, called the Endcap Timing Layer, will be instrumented with silicon Low-Gain Avalanche Diodes, covering the high-radiation pseudorapidity region $1.6 < |\eta| < 3.0$. The LGAD sensors will be read out by the ETROC readout chip, which is being designed for precision timing measurements. We present recent progress in the characterization of LGAD sensors for the Endcap Timing Layer and the development of ETROC, including test beam and bench measurements.

1. The CMS MIP timing detector

During the Large Hadron Collider (LHC) Phase-2, called High-Luminosity LHC (HL-LHC), the instantaneous luminosity will increase by a factor ∼5, leading the number of proton–proton collisions per bunch crossing up to 140–200 [1]. In this environment, the spatial overlap (pile-up) of particle tracks will increase, degrading the performances of the vertex reconstruction and particle identification in Compact Muon Solenoid (CMS) [2]. Hence the CMS collaboration approved to upgrade its detector with a MIP Timing Detector (MTD) [3] with the aim to add timing information to charge particle tracks. The MTD aims to mitigate the effects of pile-up in the Phase-2 environment to the value of Phase-1, providing a timing resolution of 30–40 ps per track.

The MTD detector will be divided into a Barrel Timing Layer (BTL) and an Endcap Timing Layer (ETL), Fig. 1. The BTL will be instrumented with LYSO Crystals coupled to Silicon Photomultipliers (SiPMs) readout by the TOFHIR ASIC, covering the pseudorapidity region $|\eta| < 1.45$, for a total surface of ∼38 m^2. The ETL will be instrumented with LGAD sensors [4,5] readout by the Endcap Timing Layer Read-Out Chip (ETROC) ASIC, covering the pseudorapidity region $1.6 < |\eta| < 3.0$, for a total surface of ∼14 m^2. The choice to instrument barrel and endcap regions with different sensor technologies is mainly due to the larger difference in area and irradiation fluences to which these regions will be exposed. In the barrel region the irradiation fluence will reach $2 \cdot 10^{14}$ n_{eq}/cm^2, while in the endcap it will exceed 10^{15} n_{eq}/cm^2.

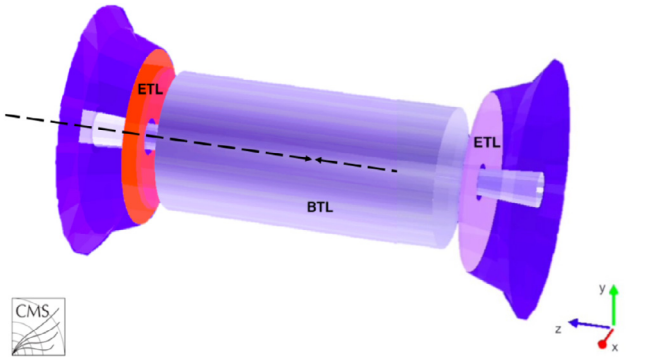

Fig. 1. A schematic view of the MTD detector, divided into a Barrel Timing Layer and an Endcap Timing Layer.

2. The MTD endcap timing layer

The ETL of the MTD detector will be mounted on the nose of the High Granularity Calorimeter, 3 m away from the interaction point. The ETL will be composed of two double-sided disks for each endcap region (four disks in total, 0.31 m < disk radius < 1.20 m), with a geometrical acceptance of ∼85 %/disk. The pairing of disks will provide two hits on most tracks, providing a timing resolution <50 ps per single hit and <35 ps per track, up to the end of ETL lifetime. The ETL will have a fill-factor (ratio between active and total detector's area) as high as possible, and low occupancy to avoid double hits and ambiguous time

E-mail address: marco.ferrero@to.infn.it.

https://doi.org/10.1016/j.nima.2022.166627
Received 3 January 2022; Received in revised form 17 February 2022; Accepted 8 March 2022
Available online 24 March 2022
0168-9002/

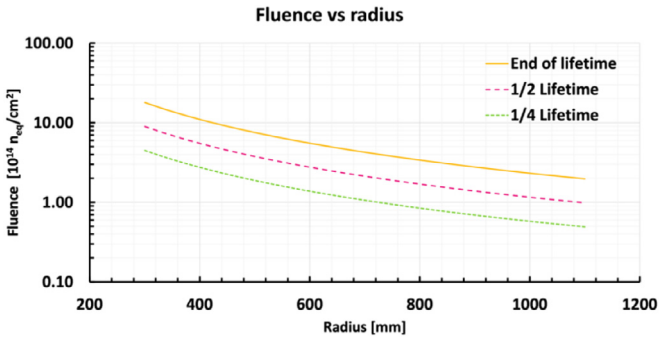

Fig. 2. Expected irradiation fluence as a function of the ETL radius for three different period of operation of the detector: 1/4 (dotted line), 1/2 (dashed line) and end of lifetime (continuous line).

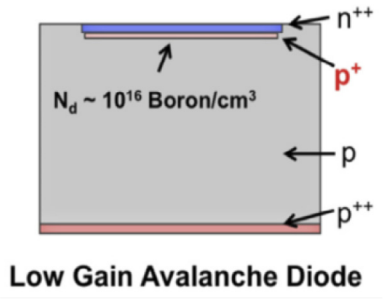

Fig. 3. A schematic view of LGAD sensor with its p^+gain layer implanted underneath the $p-n$ junction.

assignment: the required occupancy is below 0.1% at low η and ∼1% in the inner region of the detector. The ETL will operate at a temperature of −25 °C.

2.1. Radiation environment in ETL

The ETL will operate in a large range of radiation fluences, aiming to ensure unchanged timing performances up to the end of the HL-LHC program.

Fig. 2 shows the FLUKA simulated irradiation fluence in 1-MeV-neutron equivalent/cm^2 (n_{eq/cm^2}) as a function of the disk's radius, at three moments of the detector lifetime (1/4, 1/2 and 1). The fluence increases towards the inner region of disks, growing up to $1.7\cdot10^{15}$ n_{eq/cm^2} at $|\eta| = 3.0$, at the end of lifetime of the detector. This maximum expected fluence increases to $2.5\cdot10^{15}$ n_{eq/cm^2} when considering a safety factor ×1.5.

The fluence of $1\cdot10^{15}$ n_{eq/cm^2} is a benchmark for the timing performances of LGADs; below this, LGADs provide a large signal with which the desired timing resolution can be readily achieved. At higher fluences, it is more challenging to maintain large signals and special radiation-resistant LGAD designs are necessary to provide them. The fluence $1\cdot10^{15}$ n_{eq/cm^2} will be exceeded only in 12% of the detector surface, starting after about 50% of the HL-LHC expected luminosity. The ETL LGAD sensors have been designed to achieve unchanged timing performances up to the end of HL-LHC.

3. The ETL sensors

An LGAD is a n-in-p silicon sensor with a p^+ boron-doped layer, called gain layer, implanted underneath the n^{++} electrode (see Fig. 3). The gain layer has a thickness of ∼1 μm and a concentration of $\sim10^{16}$ atoms/cm^3. When the LGAD operates in reverse bias, the high p^+ concentration generates an electric field greater than 300 kV/cm into the gain layer volume. This field is high enough to start avalanche multiplication by impact ionization when charge carriers generated by particles pass through the high field region.

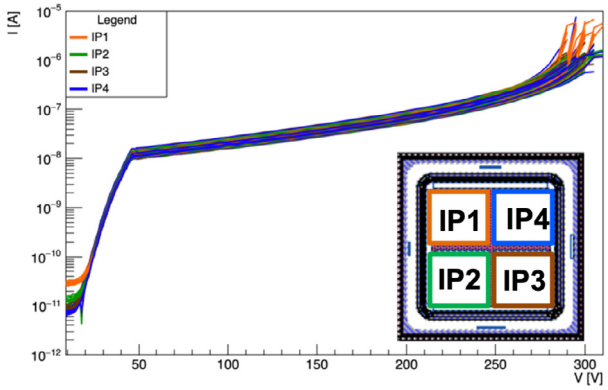

Fig. 4. Current–Voltage measurements of 25 2 × 2 LGAD sensors arrays produced by FBK. The measurements have been performed at room temperature.

LGAD sensors are designed to have a moderate internal gain, between 10 and 30, to maximize the signal to noise ratio. A large signal-to-noise ratio combined with a thin active thickness of the sensor are the key ingredients to achieve excellent timing resolution σ_t:

$$\sigma_t^2 \approx \left(\frac{N}{S/t_{rise}}\right)^2 + \sigma_{landau}^2. \quad (1)$$

The terms N and S are the noise and signal amplitude, which depends on the internal gain of the sensor as well as the characteristics of the read-out electronic. The terms t_{rise} and σ_{landau} are the rising time of the signal and the contribution to timing resolution due to Landau fluctuation (non-uniform charge deposition), both depending on the sensor active thickness, [6].

The main ETL sensor requirements are: (i) active thickness of ∼50 μm; (ii) pad capacitance below 3–4 pF; (iii) low (<μA) and uniform pad leakage current; (iv) uniformity of gain layer implants to provide uniform breakdown voltage; (v) signal greater than 8 fC (new sensors) and 5 fC (end of lifetime); (vi) per-track timing resolution of ∼ 30–40 ps. The final ETL sensor will be a 16 × 16 pad array with pads of an active area of 1.3 × 1.3 mm^2.

Large prototypes of LGADs have been produced by Fondazione Bruno Kessler (FBK) and Hamamatsu Photonics (HPK) in two R&D productions called UFSD3.2 and HPK2, respectively. Both foundries produced LGADs with several different p^+ doses and inter-pad layouts. FBK produced sensors with carbonated gain layers to improve the radiation resistance of LGAD technology [7,8]. These two productions have been extensively tested in laboratory and during beam test activity at Fermi National Accelerator Laboratory (FNAL) facility [9].

3.1. Production uniformity

A large number of LGAD sensors have been tested in laboratory using a probe station, performing DC measurements of the leakage current as a function of the bias voltage. In this way, the uniformity of FBK and HPK LGAD productions have been characterized in terms of breakdown voltage and leakage current.

Fig. 4 shows the leakage currents of each pad in 25 2 × 2 LGAD sensors arrays from a wafer of the FBK-UFSD3.2 production. These measurements show a very high uniformity of: (i) breakdown voltage (280 V < V_{BD} < 300 V); (ii) leakage current before the breakdown, which is also very low (<1 μA). Similar measurements have been performed on other wafers from the FBK-UFSD3.2 production and sensors from HPK2 production.

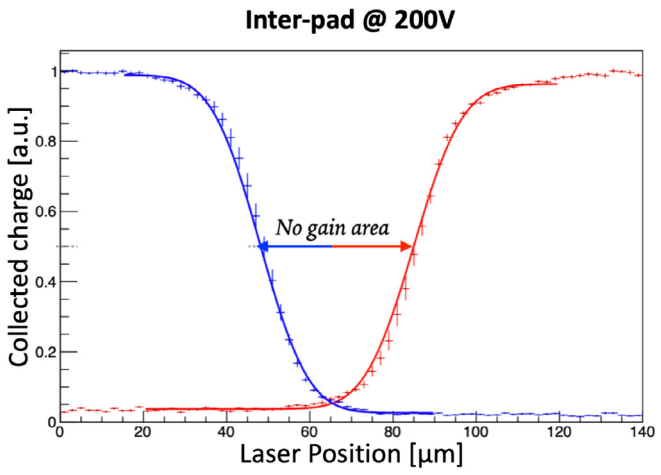

Fig. 5. Collected charge profiles on two adjacent pads of an ETL FBK-LGAD. This measurement has been obtained by performing a TCT scan across two adjacent pads. Solid lines are the fit functions given by the convolution of Step and Gaussian functions.

3.2. No-gain region distance

Another important measurement performed on LGADs is the estimation of the no-gain (inter-pad) distance between two adjacent pads. This parameter determines the fill-factor (active area on total area) of the detector, the smaller the inter-pad the better the fill-factor is. For example, for ETL sensors, inter-pads of ∼40 μm and ∼100 μm correspond to fill-factors of ∼94% and ∼85%, respectively.

This measurement was performed using the Transient Current Technique (TCT) setup developed by Particulars [10]. The TCT setup is equipped with a pulsed and focused (spot diameter ∼10 μm) infrared ($\lambda = 1064$ nm) laser, that simulates the passage of a Minimum Ionizing Particle. The LGADs under test were wire-bonded on dedicated test boards and read-out by Cividec broad-band current amplifiers. The inter-pad distance measurement has been made by performing a laser scan between two adjacent pads along optical slits, on the surface of the sensors.

The Fig. 5 shows an example of an inter-pad distance measurement performed on a new FBK-LGAD biased at 200 V. The blue and red markers define the profiles of the collected charge, obtained moving the laser spot from a pad to the adjacent one. The shape of the charge profile has been fitted with an S-curve, given by convolution of a Step function that approximates the edge region of the pad and of a Gaussian function that approximates the laser beam profile. The no-gain distance has been estimated as the distance between the two step functions, which is located at the 50% point of the S-curves.

FBK and HPK LGADs with three and four different inter-pad layouts have been characterized. No-gain distances between 35 μm and 120 μm have been measured, in agreement with the nominal inter-pad gaps. Finally, the no-gain distances in irradiated LGADs have been measured, verifying that they have not changed.

3.3. Timing resolution of LGADs

An important characterization of LGADs is the timing resolution when new and irradiated. This characterization has been performed at the University of Turin and the Fermilab SiDet Laboratory, using β-source telescopes and very low noise electronics to benchmark the sensors performances. ^{90}Sr-β-sources emitting 2 MeV β-particles have been used to test the sensors timing performances; a β-particle replicates the passage of a minimum ionizing particle, generating the same amount of charge along the active thickness of the sensor. Timing resolution has been measured at −25 °C on FBK and HPK LGADs,

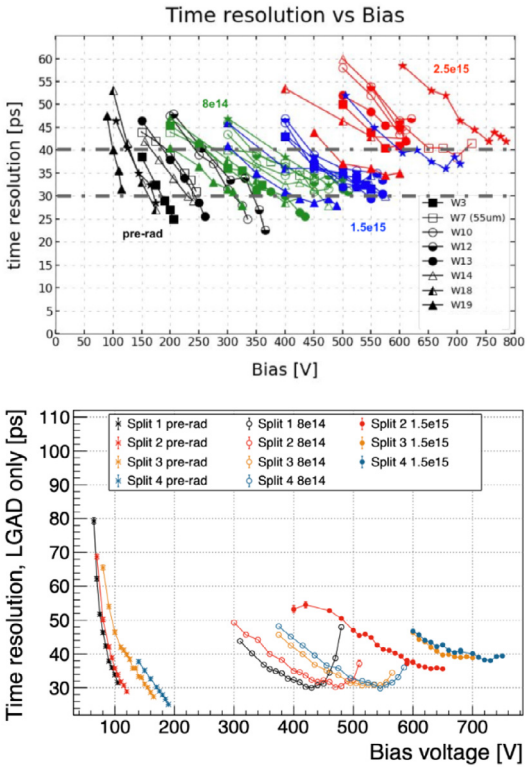

Fig. 6. Timing resolution as a function of bias voltage of FBK (top) and HPK (bottom) LGADs. On the top the FBK sensors irradiated up to $2.5 \cdot 10^{15}$ n_{eq}/cm^2: each marker type identifies a different gain layer design, while each color identifies different irradiation fluences: new; $8 \cdot 10^{14}$ n_{eq}/cm^2; $1.5 \cdot 10^{15}$ n_{eq}/cm^2; $2.5 \cdot 10^{15}$ n_{eq}/cm^2, [11]. On the bottom the HPK sensors irradiated up to $1.5 \cdot 10^{15}$ n_{eq}/cm^2, where color identify gain layer designs, while marker types identify irradiation fluences: new (star); $8 \cdot 10^{14}$ n_{eq}/cm^2 (empty circle); $1.5 \cdot 10^{15}$ n_{eq}/cm^2 (filled circle), [12].

irradiated with neutrons up to $2.5 \cdot 10^{15}$ n_{eq}/cm^2 and $1.5 \cdot 10^{15}$ n_{eq}/cm^2, respectively.

Fig. 6 reports the timing resolution measurements on FBK (top) [11] and HPK (bottom) [12] LGADs of ETL prototypes. All sensors irradiated up to $1.5 \cdot 10^{15}$ n_{eq}/cm^2 achieved a resolution below 40 ps. The FBK sensors irradiated to $2.5 \cdot 10^{15}$ n_{eq}/cm^2 were able to reach 40 ps.

All tested sensors satisfied the ETL single-hit timing resolution requirement <50 ps, including the ASIC additional contribution to the timing resolution (see Section 4).

3.4. Beam test

Several LGADs sensors has been characterized and tested at the FNAL beam test facility. The facility used a 120 GeV/c protons beam, is instrumented with a strips and pixels telescope to provide particle hit position, and a High-Speed Photek Micro-Channel Plate with a timing precision of ∼10 ps to provide timestamp [13].

An example of two measurements performed at the FNAL facility are timing resolution and hit efficiency maps on large size pad-array LGADs. Fig. 7 shows these two maps for a HPK-4 × 4 LGAD array, operated at reverse bias of 195 V to provide an amount of charge greater than 8 fC . The map on the top shows a very good uniformity of timing resolution (∼40 ps) all across the sensor active surface, while the map on the bottom shows a very uniform hit efficiency of ∼100% over the active area of the sensor, [14]. In both measurements, the no gain-region between pads is clearly visible and a width of this region in agreement with the TCT measurements has been measured [14]. These results qualify large unirradiated LGAD sensors array in term of timing resolution and efficiency performances.

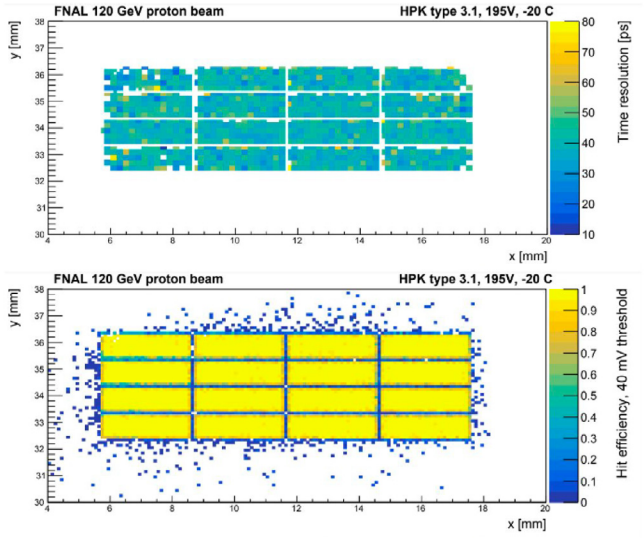

Fig. 7. Timing resolution (top) and hit efficiency (bottom) maps of a new 4 × 4 LGAD array with 3 mm^2 pads [14]. These measurements have been performed at FNAL beam test facility, at −20 C°, and biasing the sensors at a fixed voltage of 195 V (provided charge >8 fC).

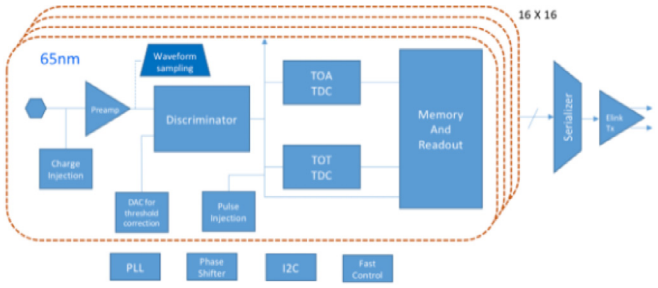

Fig. 8. Block diagram of an ETROC single channel, with a preamplifier, a discriminator and a TDC stage.

4. The ETL read-out ASIC

The ETL LGAD sensors will be read out by a new ASIC so-called ETROC, designed in 65 nm technology. The aim of the ETROC-LGAD system is to provide a timing resolution below 50 ps up to the end of the lifetime of the detector. To achieve this target ETROC needs a front-end that combines low noise with a fast rise time. The power budget is 1W/chip.

Three prototype versions of the chip are foreseen before the full-size 16 × 16 ASIC. ETROC0 and ETROC1 are the two first prototypes produced, both tested in laboratory and during beam test activity [15]. A schematic view of the block diagram of an ETROC single channel is shown in Fig. 8.

ETROC0 is a single analog channel chip based on a preamplifier and discriminator stage. Charge injection tests showed a discriminator leading-edge jitter below 20 ps, for injected charges greater than 8 fC; this result is in agreement with post-layout simulation. Moreover, ETROC0 bonded to LGAD sensor has been characterized during beam test, achieving a promising timing resolution of 31 ps and an efficiency of 100% at discriminator output.

ETROC1 is a 16 channels ASIC with integrated Time-to-Digital-Converters (TDCs) to perform Time-of-Arrival and Time-over-Threshold analysis. The TDC design has been optimized for low power, using simple delay cells with self-calibration. The front-end (preamplifier and discriminator) implemented in ETROC1 is the same as ETROC0. The timing resolution of ETROC1 bump-bonded to LGAD has been

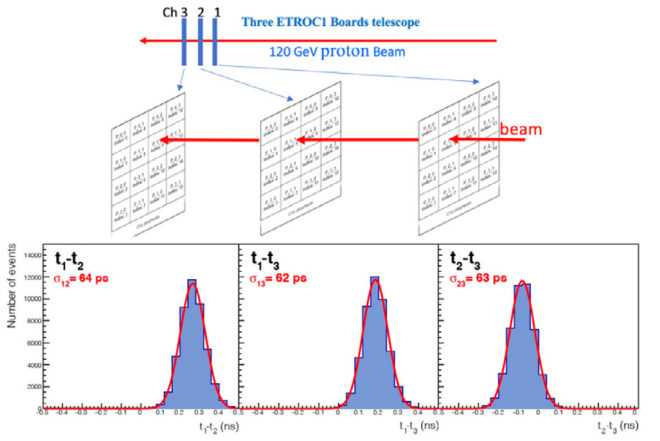

Fig. 9. Top: ETROC1 boards telescope assembled and tested during FNAL beam test. Bottom: time difference distributions of the particles time of arrivals for pairs of ETROC1 boards; 1, 2 and 3 are the indexes of the boards, while σ_{12}, σ_{13} and σ_{23} are the widths of the time difference distributions [15].

measured during beam test at FNAL, and a value of 42–46 ps has been found. The contribution of the TDC to this timing resolution has been estimated to be ∼6 ps. The timing resolution measurement of the ETROC-LGAD system has been performed using a three-plate telescope of ETROC1 boards (Fig. 9-top). Fig. 9-bottom reports the distributions of the time difference between the time of arrivals of particles for pairs of ETROC1 boards, while the widths of these distributions give the timing resolution of each pair of boards.

The third prototype of the chip will be ETROC2, which will have the full functionality and size of the final chip. This chip version will be submitted in 2022.

5. Conclusion

The CMS Endcap Timing Layer will provide time measurements of charged particles with single-hit timing resolution below 50 ps, helping the CMS detector to maintain its excellent performances in the very challenging environment of the HL-LHC. ETL will be instrumented with LGAD sensors read out by the new ETROC ASIC.

LGADs from FBK and HPK productions have been tested in laboratory and during beam tests at FNAL, with the following results: (i) the sensors showed high uniformity of leakage current and breakdown voltage proving the good uniformity of the productions; (ii) no-gain region width <120 μm have been measured in different FBK and HPK sensor layouts; (iii) irradiated LGADs showed excellent timing resolution, below 40 ps up to irradiation fluence of $2.5 \cdot 10^{15}$ n_{eq/cm^2} in FBK sensors and of $1.5 \cdot 10^{15}$ n_{eq/cm^2} in HPK ones, fulfilling the ETL requirement of 50 ps per single hit; (iv) beam test results showed uniform timing resolution (∼40 ps) and efficiency (∼100%), for amount of charge above 8 fC, all across the active area of large unirradiated LGAD sensors arrays.

The ETL Read-out chip will ensure excellent timing performances (<50 ps) while consuming 3 mW/channel. ETROC will have 256 channels. ETROC1 is the second prototype version of the chip produced and tested; this version is a 16 channels chip with the same front-end of the previous version (ETROC0) and with integrated TDCs. ETROC1 bonded to LGAD achieved a timing resolution of 42–46 ps, measured during beam test.

Declaration of competing interest

The authors declare that they have no known competing financial interests or personal relationships that could have appeared to influence the work reported in this paper.

References

[1] G. Apollinari, I.B. Alonso, O. Brüning, M. Lamomt, L. Rossi, High-Luminosity Large Hadron Collider (HL-LHC), Tech. Rep., CERN, 2015, Preliminary Design Report,

[2] CMS, The CMS experiment at the CERN LHC, J. Instrum. 3 (08) (2008) S08004, http://dx.doi.org/10.1088/1748-0221/3/08/s08004.

[3] CMS, A MIP Timing Detector for the CMS Phase-2 Upgrade, Tech. Rep., CERN, Geneva, 2019.

[4] G. Pellegrini, P. Fernández-Martínez, M. Baselga, C. Fleta, D. Flores, V. Greco, S. Hidalgo, I. Mandić, G. Kramberger, D. Quirion, M. Ullan, Technology developments and first measurements of Low Gain Avalanche Detectors (LGAD) for high energy physics applications, Nucl. Instrum. Methods Phys. Res. A 765 (2014) 12–16, http://dx.doi.org/10.1016/j.nima.2014.06.008, HSTD-9 2013 - Proceedings of the 9th International "Hiroshima" Symposium on Development and Application of Semiconductor Tracking Detectors.

[5] M. Ferrero, R. Arcidiacono, M. Mandurrino, V. Sola, N. Cartiglia, An Introduction to Ultra-Fast Silicon Detectors: Design, Tests, and Performances, 2021, http://dx.doi.org/10.1201/9781003131946.

[6] N. Cartiglia, R. Arcidiacono, M. Baselga, R. Bellan, M. Boscardin, F. Cenna, G. Dalla Betta, P. Fernndez-Martnez, M. Ferrero, D. Flores, Z. Galloway, V. Greco, S. Hidalgo, F. Marchetto, V. Monaco, M. Obertino, L. Pancheri, G. Paternoster, A. Picerno, G. Pellegrini, D. Quirion, F. Ravera, R. Sacchi, H.-W. Sadrozinski, A. Seiden, A. Solano, N. Spencer, Design optimization of ultra-fast silicon detectors, Nucl. Instrum. Methods Phys. Res. A 796 (2015) 141–148, http://dx.doi.org/10.1016/j.nima.2015.04.025, Proceedings of the 10th International Conference on Radiation Effects on Semiconductor Materials Detectors and Devices.

[7] M. Ferrero, R. Arcidiacono, M. Barozzi, M. Boscardin, N. Cartiglia, G.D. Betta, Z. Galloway, M. Mandurrino, S. Mazza, G. Paternoster, F. Ficorella, L. Pancheri, H.-F.W. Sadrozinski, F. Siviero, V. Sola, A. Staiano, A. Seiden, M. Tornago, Y. Zhao, Radiation resistant LGAD design, Nucl. Instrum. Methods Phys. Res. A 919 (2019) 16–26, http://dx.doi.org/10.1016/j.nima.2018.11.121.

[8] M. Ferrero, Radiation resistant LGAD design, in: 16th "Trento" Workshop on Advanced Silicon Radiation Detectors, TREDI, 2021.

[9] https://ftbf.fnal.gov/.

[10] http://particulars.si.

[11] F. Siviero, Characterization with a β-source setup of the UFSD3.2 production manufactured at FBK, in: 16th "Trento" Workshop on Advanced Silicon Radiation Detectors, TREDI, 2021.

[12] R. Heller, The CMS MIP timing detector, in: 5th Technology and Instrumentation in Particle Physics conference, 2021.

[13] S. Kwan, C. Lei, D. Menasce, L. Moroni, J. Ngadiuba, A. Prosser, R. Rivera, S. Terzo, M. Turqueti, L. Uplegger, L. Vigani, M.E. Dinardo, The pixel tracking telescope at the Fermilab Test Beam Facility, Nucl. Instrum. Methods Phys. Res. A 811 (2016) 162–169, http://dx.doi.org/10.1016/j.nima.2015.12.003.

[14] R. Heller, A. Abreu, A. Apresyan, R. Arcidiacono, N. Cartiglia, K. DiPetrillo, M. Ferrero, M. Hussain, M. Lazarovitz, H. Lee, S. Los, C. Moon, C. Peña, F. Siviero, V. Sola, T. Wamorkar, S. Xie, Combined analysis of HPK 3.1 LGADs using a proton beam, beta source, and probe station towards establishing high volume quality control, Nucl. Instrum. Methods Phys. Res. A 1018 (2021) 165828, http://dx.doi.org/10.1016/j.nima.2021.165828.

[15] G. Oh, ETROC project for the CMS MTD Endcap Timing Layer (ETL), in: Meeting of the Division of Particles and Fields of the American Physical Society, DPF21, 2021.